# Chemical bond and electronic states in calcium silicides: Theory and comparison with synchrotron-radiation photoemission

O. Bisi
*Dipartimento di Fisica dell'Università degli Studi di Modena, via Campi 213/A, Modena, Italy*

L. Braicovich,* C. Carbone,† and I. Lindau
*Stanford Electronics Laboratories, Stanford University, Stanford, California 94305-4055*

A. Iandelli, G. L. Olcese, and A. Palenzona
*Istituto di Chimica Fisica dell'Università degli Studi di Genova, Corso Europa 1, I-16145 Genova, Italy*
(Received 24 January 1989; revised manuscript received 1 June 1989)

We present a combined theoretical and experimental investigation of the electron properties of calcium silicides ($Ca_2Si$, CaSi, and $CaSi_2$). The theoretical study is performed by a self-consistent calculation of the electron states, while the experimental analysis is based on synchrotron-radiation photoemission measurements. The overall agreement between the computed and measured spectra allows us to investigate the main features of the Ca-Si interaction in different compounds. We find that covalent character is present in the Ca—Si bond and that the strength of this interaction increases with Si concentration. Furthermore all the Ca *s-p-d* states are involved in this coupling with Si. In $Ca_2Si$, the Si *s* states are found in a corelike configuration, while in the other compounds they are promoted to form an *s-p* valence band. The covalent interaction is not sufficient to interpret the results and some ionic character is present in the Ca—Si bond. $Ca_2Si$ is found to be a semimetal and many structures in the density of states can be correlated to well-defined interactions between the nonequivalent Ca-Si couples that are found in these complex compounds.

## I. INTRODUCTION

The study of the electron states of silicides has received much attention in recent years. This is due both to the interest in the problem itself and to its connection with interface physics: In fact, many silicon-metal interfaces are reactive and the interface silicide-like products control the electronic properties of the junction; therefore studies of the electron states of silicides are connected both with fundamental problems and with the perspective of a deeper understanding of the associated technological problems.

In the study of the electron states and of the chemical bond of transition-metal silicides, the first breakthrough has been the description in terms of the hybridization between metal *d* and silicon *p* states in the frame of a two-level model.[1,2] This treatment can successfully explain the gross features of photoemission experiments on near-noble silicides[3–10] on some refractory-metal silicides[11,12] as well as trends across the series of 3*d*-metal silicides.[13] For an extensive summary of these subjects see Ref. 14.

This model must be regarded, however, as a first approximation which is useful to point out the general features of the chemical bond such as the importance of covalency, but which is not sufficient for a detailed comparison between theory and experiments. A number of first-principles calculations using real crystal structures have shown that the experimental results cannot be interpreted solely in terms of the two-level model.[15–18] These calculations allow one to go deeper into the problem concerning the contribution of the atomic states to the chemical bond and to sort out the features of the electron structures, which depend upon the characteristics of the crystal structure, such as the role of nonequivalent atoms of the same species.

The present paper and the following one must be considered in this larger perspective: We present extensive calculations of the electron states of all the Ca silicides carried out with the Andersen linear muffin-tin orbital (LMTO) method in the atomic-sphere approximation[19] (ASA) and we compare the results for occupied states with synchrotron-radiation photoemission (in the present paper, I) and the results for empty states with inverse photoemission in the ultraviolet region (next paper,[20] hereafter referred to as paper II). In both cases experiments have been performed on polycrystalline samples; the comparison with theoretical results takes into account the experimental sensitivity to the different density-of-states contributions. Since the LMTO eigenvalue $E$ has errors of fourth and higher order in $E-E_\nu$ with respect to the fixed but arbitrary energy $E_\nu$ we present two sets of calculations. The results presented in this paper are computed with $E_\nu$ fixed at the center of the occupied part of the bands, while in the calculations presented in paper II $E_\nu$ is fixed in the empty-state region. This allows us to describe a $\sim$24-eV-wide energy range well. The negligible difference between the results presented in the two papers gives evidence of the accura-

 

cy of our results.

Due to their low $d$ occupancy, Ca silicides are the best candidates for a study beyond the two-level model: the center of the Ca $d$ band is, in fact, located ~4–6 eV above the Fermi energy and the mixing between Ca $d$ and Si $p$ states cannot be the only relevant bonding interaction. Furthermore, the difference in electronegativity between Ca and Si, 0.9 according to Pauling's scale, suggests that ionicity would play a fundamental role in the bonding. The relevance of an ionic contribution of the Si—Ca bond has also been shown by Franciosi *et al.*,[21] but the above arguments do not interpret the nature of the bond in these compounds; on the contrary, they point out the importance of a detailed study of their electronic properties.

Other specific reasons to investigate Ca silicides are presented in the following. The region of low $d$ occupancy also includes, besides the other elements of column II, the rare-earth silicides, which are an important family in interface physics.[22,23] Calcium silicides can be considered prototypes of this family and of Si–rare-earth interfaces in the study of processes like the Si $L_{2,3}$ Auger transition.[24,25] In the field of interface physics, a good knowledge of Ca silicides is obviously useful to discuss the interfaces with column-II elements such as Si/Ca interfaces,[21,26] Si/Ba interfaces,[27] and related systems such as Si/Y.[28] The interface between Si(111) and Ca appears to be quite promising since it is possible to grow epitaxial $CaSi_2$ films by annealing the Ca metal deposited onto clean Si(111) substrate. In this respect $CaSi_2$ is similar to $CoSi_2$ and $NiSi_2$, the only other systems which yield single-crystal interfaces which are atomically abrupt and atomically smooth over extended regions. The fundamental reason for this similar behavior of such different systems is not known at present and deserves accurate investigations particularly on the role of $d$ states and on the covalent-ionic character of the Si-metal bond. Furthermore, a better understanding of the Si-Ca interaction is of strong interest in connection with the problem of $Si/CaF_2$ interfaces, a problem which is receiving considerable attention due to the formation of an epitaxial semiconductor, large-band-gap insulator interface.[29–31] Very recently,[32] it has been shown that the $Si/CaF_2$ interface is not abrupt, but is mediated by a $CaSi_2$-type layer which is deficient in F. Again, the features of the Ca—Si bond are essential to understand this unique interface structure.

We conclude by mentioning that this paper and the following one are the first systematic accounts of these calculations and of photoemission (direct and inverse); a very preliminary report has been presented[33] and bremsstrahlung isochromat spectra in the x-ray region from two silicides (CaSi and $CaSi_2$) have been published;[34] the effects of correlation in core-valence-valence Auger transitions from Si $2p$ excitation have been discussed in Ref. 35. The paper is organized as follows. The structure of the silicides is given in Sec. II, the method of calculation is presented in Sec. III, and the experimental methods are given in Sec. IV. The theoretical results are discussed in detail in Sec. V, while the calculations are compared with the experiment in Sec. VI and the conclusions are summarized in Sec. VII.

## II. THE STRUCTURE OF Ca SILICIDES

The fundamental data concerning the Ca-silicides crystal structure[36] are listed in Table I. It is evident that these compounds form complex structures with many atoms per unit cell. Furthermore, in $Ca_2Si$ and $CaSi_2$ there are two nonequivalent Ca [Ca(1) and Ca(2)] and Si [Si(1) and Si(2)] atoms, respectively.

The Bravais lattice is simple orthorhombic in $Ca_2Si$, base-centered orthorhombic in CaSi and trigonal in $CaSi_2$. The coordination numbers and the interatomic distances of Ca and Si atoms in these three compounds are displayed in Table II. The most remarkable fact concerning $Ca_2Si$ is that the Ca(2) atom has only three Si neighbors below 3.5 Å (3.11–3.27 Å), while the Ca(1) atom has four Si neighbors in the range 2.97–3.08 Å. Furthermore, the CA neighbors of Ca(2), at distances greater than 3.6 Å, are located farther than the corresponding Ca neighbors of Ca(1). The consequences of these geometrical differences will be examined in the section dedicated to the analysis of the electronic structure.

As far as $CaSi_2$ is concerned, it should be noticed that a Ca atom corresponding to the one found at a distance of 3.11 Å from Si(1) is missing in the Si(2) case. Again, this feature will be responsible for characteristic structures in the projected density of states.

TABLE I. Crystal geometry and structural information for Ca silicides.

| | |
|---|---|
| $Ca_2Si$ | Bravais lattice: simple orthorhombic |
| | Space group: $Pnma$ (62nd) |
| | $\Omega_{cell}=330.871$ Å$^3$ |
| | $a=7.667$ Å |
| | $b=4.799$ Å |
| | $c=9.002$ Å |
| | 4 molecules per cell |
| | 2 nonequivalent Ca atoms per cell |
| | Packing fraction $f=0.67$ |
| CaSi | Bravais lattice: base-centered orthorhombic |
| | Space group: $Cmcm$ (63rd) |
| | $\Omega_{cell}=96.844$ Å$^3$ |
| | $a=4.590$ Å |
| | $b=10.795$ Å |
| | $c=3.910$ Å |
| | 2 molecules per cell |
| | Packing fraction $f=0.73$ |
| $CaSi_2$ | Bravais lattice: trigonal |
| | Space group: $R\bar{3}m$ (166th) |
| | $\Omega_{cell}=132.249$ Å$^3$ |
| | $a=10.4$ Å |
| | $\alpha=21°30'$ |
| | 2 molecules per cell |
| | 2 nonequivalent Si atoms per cell |
| | Packing fraction $f=0.59$ (no empty spheres) |
| | Packing fraction $f=0.65$ (with empty spheres) |

TABLE II. Coordination numbers and interatomic distances (in Å) for Ca silicides.

| | | | | | |
|---|---|---|---|---|---|
| | | $Ca_2Si$ | | | |
| Ca(1) | | Ca(2) | | Si | |
| 1 Si | 2.97 | 1 Si | 3.11 | 1 Ca(1) | 2.97 |
| 2 Si | 2.98 | 2 Si | 3.27 | 2 Ca(1) | 2.98 |
| 1 Si | 3.08 | 2 Si | 3.54 | 1 Ca(1) | 3.08 |
| 2 Ca(2) | 3.56 | 2 Ca(1) | 3.56 | 1 Ca(2) | 3.11 |
| 2 Ca(2) | 3.57 | 2 Ca(1) | 3.57 | 2 Ca(2) | 3.27 |
| 1 Ca(2) | 3.60 | 1 Ca(1) | 3.60 | 2 Ca(2) | 3.54 |
| 2 Ca(1) | 3.63 | 1 Ca(1) | 3.73 | | |
| 1 Ca(2) | 3.73 | 2 Ca(2) | 3.99 | | |
| | | 2 Ca(2) | 4.06 | | |
| | | CaSi | | | |
| Ca | | | | Si | |
| 4 Si | 3.11 | | | 2 Si | 2.47 |
| 1 Si | 3.13 | | | 4 Ca | 3.11 |
| 2 Si | 3.23 | | | 1 Ca | 3.13 |
| 2 Ca | 3.60 | | | 2 Ca | 3.23 |
| 4 Ca | 3.84 | | | | |
| 2 Ca | 3.91 | | | | |
| | | $CaSi_2$ | | | |
| Ca | | Si(1) | | Si(2) | |
| 3 Si(2) | 2.98 | 3 Si(1) | 2.51 | 3 Si(2) | 2.52 |
| 3 Si(1) | 2.99 | 3 Ca | 2.99 | 3 Ca | 2.98 |
| 1 Si(1) | 3.11 | 1 Ca | 3.11 | 3 Ca | 3.82 |
| 6 Ca | 3.86 | 3 Ca | 4.90 | 3 Ca | 4.89 |
| | | 6 Ca | 4.97 | | |

## III. METHOD OF CALCULATION

The complex structure of Ca silicides can be investigated through a first-principles calculation by using the efficient computational scheme offered by Andersen's linear muffin-tin orbital (LMTO) method[19,37] In the atomic-sphere approximation (ASA) the interstitial region of the muffin-tin starting potential is "annihilated" through the expansion of the muffin-tin spheres and the neglect of the slight overlap.[19] The muffin-tin spheres in this approximation thus become the Wigner-Seitz spheres which fill all the space. The potential is taken to be spherically symmetric within the spheres.

This approximation is valid for closely packed solids, i.e., when the touching sphere's interstitial region $\Omega - \Omega_0$ is less than (of the order of) $\frac{1}{3}$ of the total volume $\Omega$. In terms of the packing fraction $f = \Omega_0/\Omega$, this corresponds to $f \geq 0.67$. In $Ca_2Si$ and in CaSi it is possible to reach a satisfactory packing of the solid, as shown in Table I, by a proper choice of the Ca and Si radii. The resulting size of the Si spheres is 1.37 Å for both compounds. The radii of the Ca spheres are 2.05 Å in $Ca_2Si$ and 2.08 Å in CaSi. As we will discuss later, this choice overestimates the space region occupied by Ca atoms and this causes problems in defining the charge transfer (see also below), but does not prevent one from obtaining reliable electron states or discussing the main features of the chemical bond.

As shown in Table I, it is not possible to get a satisfactory packing in $CaSi_2$ by simply using Ca and Si spheres since this compound is characterized by various empty-space regions, like Si in the diamond lattice. It is now well established that the open structures like Si can be investigated by the LMTO ASA method by adding empty spheres to the lattice of real atoms.[38,39] Empty spheres have been introduced as ficitious atoms with zero atomic number to be placed on void sites in order to obtain the close-packing necessary for the muffin-tin approximation.[40] In $CaSi_2$ the void sites are located between Si planes. We added one empty sphere of radius 1.35 Å between Si(1) planes and a second one of radius 0.78 Å between Si(2) planes. The smaller size of the second sphere is due to the presence of Ca atoms beyond the Si(2) layers, just on the top of the void sites. In this way we are able to obtain the good packing shown in Table I. The radii of the Si(1), Si(2), and Ca spheres are 1.32, 1.30, and 2.14 Å, respectively.

The LMTO ASA band-structure calculation presented here uses the "frozen-core" approximation, i.e., the inner-electron wave functions are taken from the self-consistent atomic calculations, and only the valence states are adjusted during the self-consistent cycles. The self-consistent crystal potential computed in this way is a very good approximation to the crystal potential, since the core-state charge densities, unlike the core-state energies, do not vary appreciably on moving from the atomic to the solid-state configuration. By using this approximation the basis set is limited to Ca and Si valence *s*, *p*, and *d* wave functions, with a strong simplification of the computational procedures. The LMTO ASA frozen-core po-

tential is an all-electron potential and it is possible to compute from it core-level energies. This calculation has already been performed for Ni compounds and the computed core energies are in excellent agreement with the experimental data.[41,42] A similar calculation of Ca and Si core energies, starting from our potentials, is in progress. These results will be used to interpret the very interesting measured behavior of Ca and Si core energies in a planned forthcoming paper.[43]

Exchange and correlation contributions to both atomic and crystalline potential have been included through the Hohenberg-Kohn density-functional description in the Kohn-Sham local-density approximation.[44–46]

The $k$-integrated functions have been evaluated by the Jepsen-Andersen linear tetrahedron method[47] on a grid of 140 ($Ca_2Si$) and 147 (CaSi, $CaSi_2$) $k$ points in an irreducible part of the Brillouin zone (BZ). In the tetrahedron method the $k$-point grid where eigenvalues are computed defines a set of tetrahedral microzones. The contribution of each microcell to the density of states is computed from a linear interpolation based on the energies at the corners of the microzone, for each band.

## IV. EXPERIMENTAL PROCEDURE

The photoemission measurements were taken at the so-called "Old Grasshopper" beamline (beamline I-1) at the Stanford Synchrotron Radiation Laboratory (SSRL); the monochromator allowed to work between 65 and ~600 eV. The angle-integrated photoemission spectra were measured with a double-pass cylindrical mirror analyzer; the total linewidth of the apparatus was ~0.4 eV at 150 eV. The Fermi-level position has been checked periodically by measuring the valence edge of gold evaporated *in situ*.

The polycrystalline samples were prepared by melting stoichiometric amounts of Ca and Si in tantalum crucibles in inert-gas atmosphere. The structure of the samples was checked with x-ray diffraction. The extra phases were below 3% in $Ca_2Si$ and CaSi, and negligible in $CaSi_2$. The samples were cleaned *in situ* by scraping with a diamond file. The nature of the surfaces prepared in this way was investigated in a separate experiment with a scanning Auger system (lateral resolution 2000 Å) where samples from the same ingots were cleaned with the same procedure. The surfaces of $CaSi_2$ became totally clean; in $Ca_2Si$ and CaSi it has been found that some oxygen signal comes from a tiny fraction of the sample surface. Thus the measured photoemission spectra contain a superposition of the spectrum of the clean substance and a minor contribution from slightly contaminated regions which give rise, as shown below, to a small feature due to oxygen 2$p$. It is very important to stress that this oxygen signal comes from spatially localized regions and it is not representative of oxygen dissolved in the sample; this also ensures that the spectra from $Ca_2Si$ and CaSi are fully representative of the clean substance apart from the weak oxygen 2$p$ feature.

## V. THEORETICAL RESULTS

### A. Total energy and related quantities

In our LMTO calculation total energy is a direct output, and therefore the cohesive energy, i.e., the total energy of the atom minus the total energy of the solid, can be evaluated. It is well known that the local-density approximation (LDA) yields good results for the cohesive energies of metals if the same exchange-correlation approximation in both atomic and solid-state calculations is applied.[48] Both the Williams-Küber-Gelatt augmented-spherical-wave method of Ref. 48 and the LMTO ASA are quite successful in describing structural properties,[49] in spite of the peculiar approximations of the methods, particularly the use of nonoptimized sphere radii. The ASA approximation works well for close-packed solids, but some caution is necessary in open structures like $CaSi_2$. The inclusion of empty spheres allows one to extend the calculation to open structures. For example, the computed LMTO ASA cohesive energy of Si is 4.8 eV/atom, compared to the experimental value of 4.66 eV/atom.[38] In the calculation of Ref. 38, the presence of a second sublattice of empty spheres provides an acceptable packing fraction, $f=0.68$, similar to our values of Table I. From this point of view, the accuracy of our results is similar to that of Ref. 38; the only substantial difference between the two calculations is our neglect of the combined-correction term,[19] which corrects for the finite number of terms in the angular-momentum expansion and for the nonspherical shapes of the *cells*. In order to quantify the effect of this difference, we observe that in the case of palladium two total-energy calculations, with and without the combined-correction term, have been performed.[50] The result is that the total-energy minimum computed with (without) the combined-correction term is located at a lattice constant almost equal to (0.06 Å lower than) the measured value. The effect of the inclusion of the combined-correction term in Pd is to lower the total energy at the experimental lattice constant of ~0.15 eV/atom. Since our calculations are performed at the experimental lattice constants, this energy difference may also estimate the order of magnitude of the uncertainty in our calculation with respect to that of Ref. 38.

The computed total energies of the valence electrons are shown in Table III. Their values are given in eV/atom, i.e., the total energy of the cell has been divided by its number of atoms. These units are proportional to kilocaleries per mole through a factor of 23.06$n$, where $n$ is the number of atoms per molecule. The total valence energies for Ca and Si isolated atoms are also shown. Since the cohesive energy is calculated within the frozen-core approximation, as in Ref. 38, core energies cancel when subtracting atomic from crystal energies.

By comparing the Ca-silicides cohesive energies with the experimental values of pure Ca and Si crystals,[51] we find that the silicide values are intermediate between the pure constituents. In order to see if compound formation may take place from the energetic point of view, the heat of formation must be evaluated. Since heats of formation

TABLE III. Computed total energies, cohesive energies, and heats of formation of Ca silicides. All the data are normalized to units of eV/atom.

| | Energy (eV/atom) | | | | |
|---|---|---|---|---|---|
| | Ca | Si | $Ca_2Si$ | CaSi | $CaSi_2$ |
| Solid: total valence energy | | | −51.341 | −66.183 | −80.491 |
| Free atom: total valence energy | −19.305 | −105.298 | | | |
| Solid: cohesive energy | 1.83[a] | 4.66[a] | 3.372 | 3.882 | 3.857 |
| Solid: computed heat of formation | | | −0.599 | −0.637 | −0.140 |
| Solid: measured heat of formation | | | −0.723 | −0.781 | −0.520 |

[a]Experimental values (Ref. 51).

are 1 order of magnitude smaller than the cohesive energies, their evaluation is much more critical. Our very crude estimate of the heat of formation is obtained by subtracting the (computed) cohesive energy of the silicide phase from the (experimental) cohesive energy of Si and Ca, in the correct stoichiometric ratio. If the heat of formation is negative, compound formation takes place. Table III lists the computed heats of formation and the experimental values,[52] determined at room temperature. The comparison shown in Table III is very encouraging, since not only the magnitude, but even the trend on varying the Si content, is well described.

### B. Electronic structure and the chemical bond

The analysis of the microscopic properties of Ca silicides and the main features of the chemical bond in these compounds may be primarily obtained from the total density of states (DOS) shown in Fig. 1. Since the curves are normalized to units of states/eV atom, they may be directly compared, in spite of the different number of atoms per unit cell.

The presented DOS's are considerably different from those calculated for model structures,[13] showing that the real crystal structure must be fully taken into account.

Starting from the $Ca_2Si$ case, we see that the filled portion of the DOS consists of two bands separated by a gap of 3.5 eV. The higher-binding-energy (BE) feature is located around −7 eV, while the wider and more structured filled band lies between −3 eV and $E_F$. At the Fermi level the density of states shows a sharp minimum (see Table IV). The analysis of the band structure of this compound shows that a ~1-eV direct energy gap between the occupied and empty states is always present, except in a few $k$ points where the empty states lie below the Fermi level. From this originates the almost zero density-of-states result of Table IV, characteristic of sem-

TABLE IV. Electronic configuration and density of states at $E_F$ for Ca silicides.

| | $Ca_2Si$ | CaSi | $CaSi_2$ |
|---|---|---|---|
| Ca $s$ electrons | 0.54 | 0.45 | 0.40 |
| Ca $p$ electrons | 0.74 | 0.74 | 0.73 |
| Ca $d$ electrons | 0.72 | 0.81 | 0.87 |
| Si $s$ electrons | 1.69 | 1.60 | 1.63 |
| Si $p$ electrons | 2.29 | 2.27 | 2.24 |
| Si $d$ electrons | 0.02 | 0.12 | 0.13 |
| DOS at $E_F$ (states/atom eV) | 0.001 | 0.399 | 0.304 |

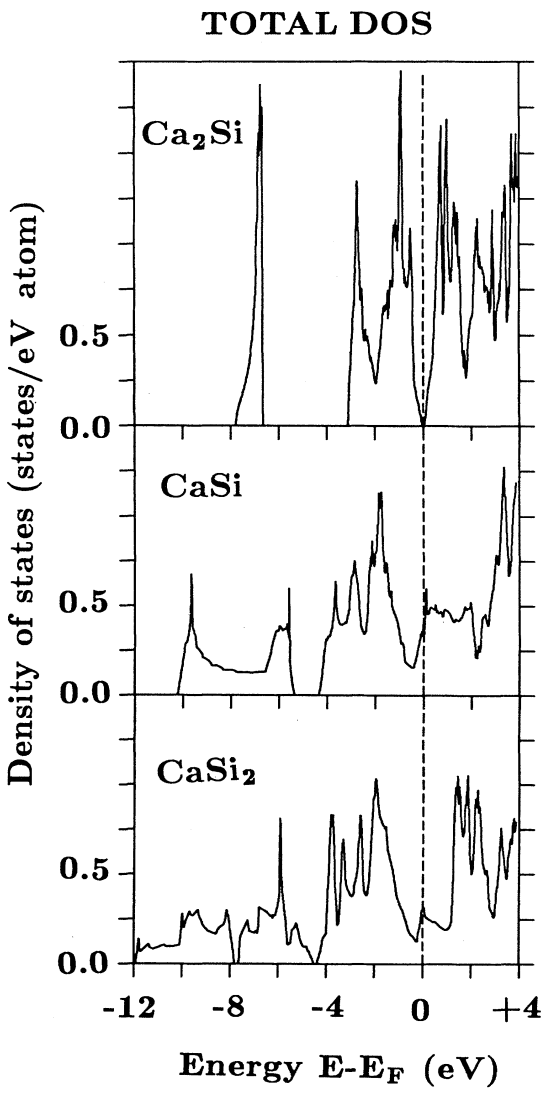


FIG. 1. Total density of states of Ca silicides.

imetallic behavior. We regard this result, i.e., a very small DOS at $E_F$, as independent of the approximations involved in the calculation. Indeed, the presence of a $\sim$1-eV gap and the shape of the bands around the Fermi level are expected to depend weakly on the computational procedure and approximations. The major source of error in the gap is expected to be the LDA, which is known to reduce the gap size.

Important modifications take place upon increasing the Si content. The most evident is the widening of the higher-BE band, whose bottom shifts down in energy, reaching $-12$ eV in $CaSi_2$. The top of this band moves up so that the internal gap is reduced to 1 eV in CaSi and to $\sim 0$ in $CaSi_2$. As a consequence of this widening, which is due to the increased Si-Si interaction, the higher-BE band becomes more structured with two well-defined peaks in CaSi, which in $CaSi_2$ give rise to two sets of bands separated by a small gap.

Even the second structure, nearer to $E_F$, turns out less

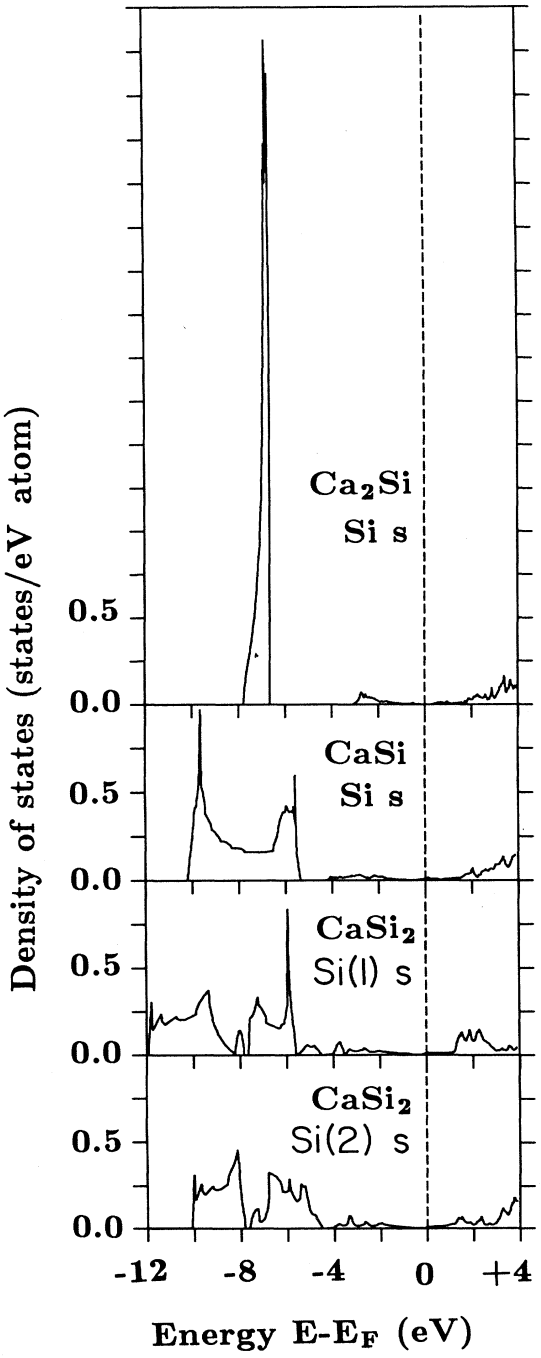


FIG. 2. Density of states of Ca silicides projected on the Si $s$ orbital.

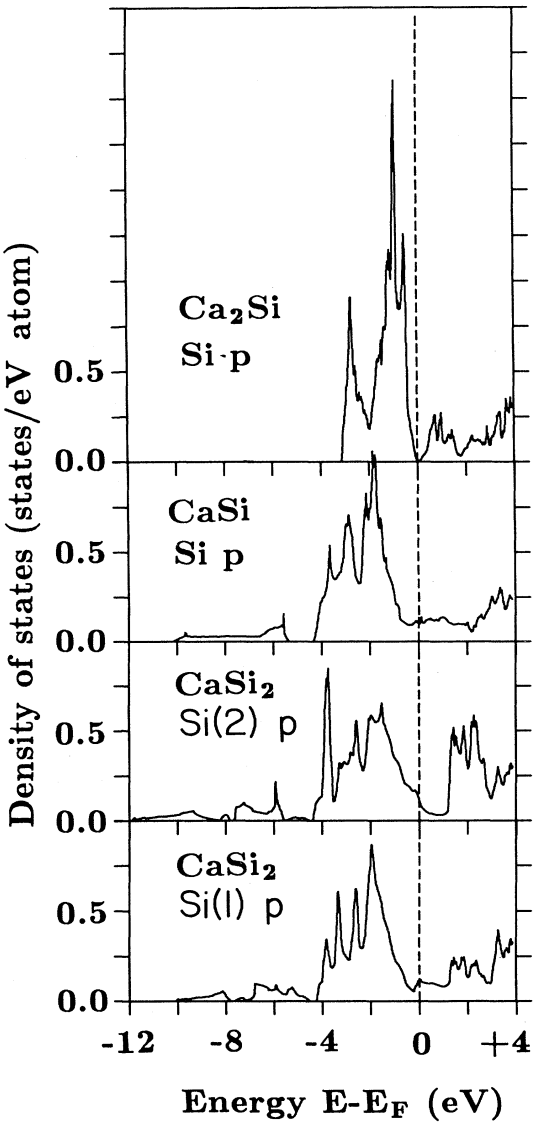


FIG. 3. Density of states of Ca silicides projected on the Si $p$ orbital.

peaked and wider in CaSi and $CaSi_2$. A dramatic change occurs in the DOS at $E_F$ that increases in CaSi and $CaSi_2$ by 2 orders of magnitude. An explanation of this effect, which is expected to have many consequences in the electrical and thermal properties of the Ca-Si system, can be obtained by looking at the electron configurations of Ca atoms shown in Table IV. The significant result is the presence of nearly one $d$ electron among the occupied states of Ca silicides. Upon going from $Ca_2Si$ to $CaSi_2$, the $d$ occupancy increases and the accompanying downward shift of the $d$ band leads to the observed strong variations of the DOS at $E_F$. We will see that this trend is due to the increasing Ca-Si interaction upon increasing the Si content.

The nature of the various features present in the DOS curves of Fig. 1 may be investigated by looking at the various angular-momentum components of the density of states projected on the Ca and Si spheres. The projected densities of states (PDOS) are displayed in Figs. 2–6. The site projection depends on the partitioning of the space region associated with a given atom, which in the solid state is somewhat arbitrary. In the LMTO ASA the partitioning is determined by the spheres enlcosing the different atoms, particularly by their relative ratio. The site-projected DOS's and their integral up to $E_F$, i.e., the associated charge, depends on this ratio. While, in principle, the sphere radii are fixed by minimizing the total energy, in practice there exists a range of possible radii which fulfill the requirements of the LMTO ASA approach, leading to the same one-electron energies, similar wave functions, but different charge transfers. Therefore the data of Figs. 2–6 preserve the basic physical information needed in order to investigate the nature of the electron states, but the charge transfer turns out to be meaningless. Since Ca silicides show very complex structures and a lattice structure intermediate between close-packed and open solids, we chose the sphere radii with the criteria of a good packing, with a packing fraction $f=\Omega_0/\Omega \geq 0.67$. In this way we obtain the values presented in Sec. III, with a Ca radius larger than the Si one. This choice obviously yields a large value of charge within the "Ca sphere," similar to that found by Nagel *et al.*[53] in $Ca_xAl_{1-x}$ metallic glasses, which can hardly be attributed to a physical charge transfer from Si to Ca. Our analysis of the valence-state properties will show that a charge-transfer picture can be applied to interpret some results. Actually, this picture implies that some charge transfer from Ca to Si takes place, as expected

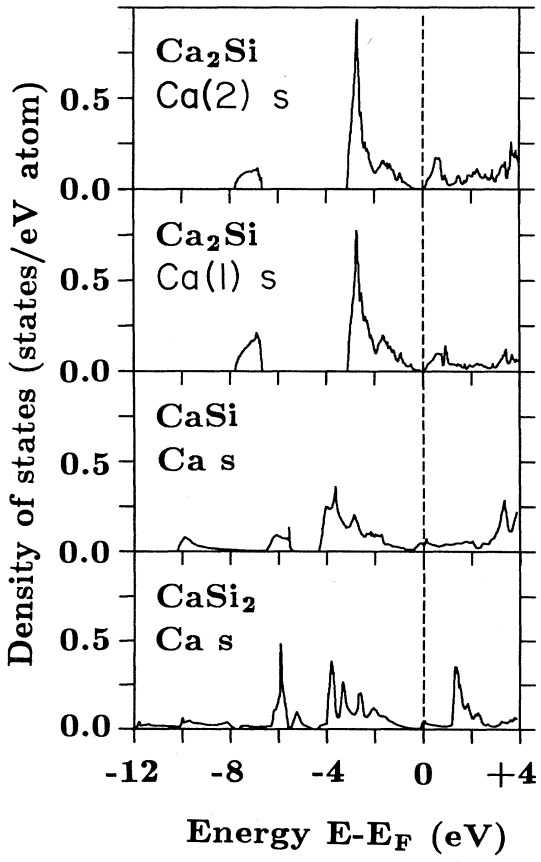


FIG. 4. Density of states of Ca silicides projected on the Ca $s$ orbital.

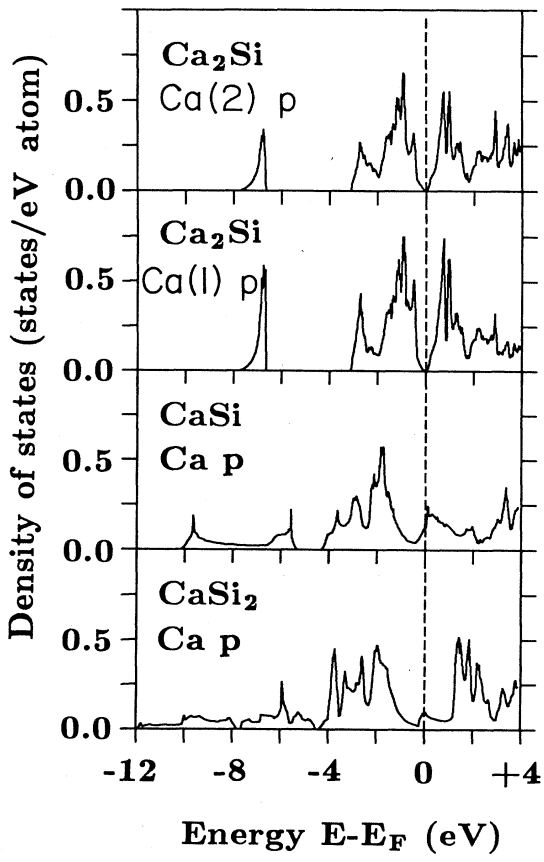


FIG. 5. Density of states of Ca silicides projected on the Ca $p$ orbital.

from the difference in electronegativity. In the following we will present the results of our calculation for each compound, deferring the comparison to the experimental data to Sec. VI.

### 1. $Ca_2Si$

Si $s$-state character is predominant in the lower-BE structure for all compounds. In $Ca_2Si$ we approach the limit of a pure Si $s$ band, since the Si $s$ band is only weakly coupled with Ca states. In this case the Si configuration is $s^2p^2$ as opposite to the diamond-structure $sp^3$ configuration, where the $3s$ orbitals have an important contribution to the bonding. This quasiatomic Si band is responsible for the strong correlation effect ($U \sim 3$ eV) found in the Si $L_{2,3}VV$ Auger process involving Si $3s$ states in this compound.[35] In this respect the picture of $Ca_2Si$ is similar to that found in many late transition-metal silicides,[1,2,13] where Si is found nearer to the atomic $s^2p^2$ than to the crystal $sp^3$ configuration. These investigations interpreted the main features of the chemical bond in many silicides as being due to the coupling between transition-metal $d$ states and the dehybridized Si $p$ orbitals. This interaction leads to the formation of $d$-$p$ bonding and antibonding states straddling the main portion of the $d$ states. These states do not participate appreciably in the bond with Si atoms (nonbonding configuration), but rather form a band mainly due to metal-$d$–metal-$d$ interaction, as in the pure transition metal.

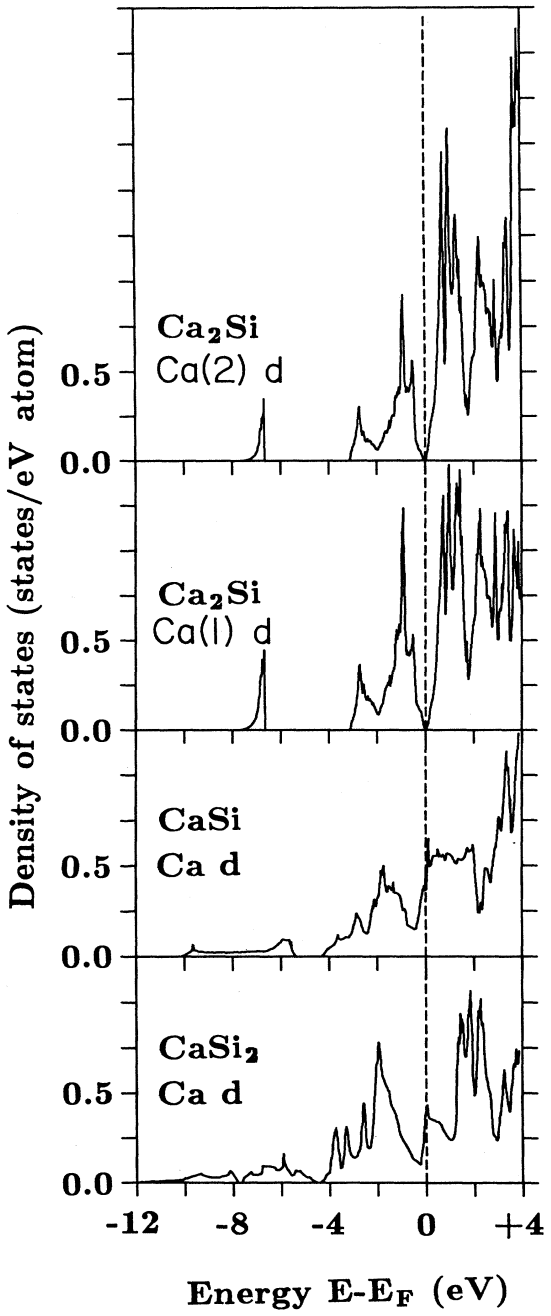


FIG. 6. Density of states of Ca silicides projected on the Ca $d$ orbital.

It is not obvious if this simple picture is valid in Ca silicides, where the metal $d$ band is mainly in the unoccupied part of the spectrum. Figure 6 shows that the Ca $d$ states form a well-defined structure in the occupied part of the spectrum. This result is different from what happens in metallic calcium, where only a tail of the main $d$ band is occupied[54,55] and is due to the bonding interaction with silicon. The electron configuration of Ca in $Ca_2Si$ is $s^{0.54}p^{0.74}d^{0.72}$ (Table IV), to be compared with the configuration of metallic calcium,[56] $s^{0.85}p^{0.66}d^{0.48}$. From this point of view, Ca silicides are similar to late-transition-metal silicides. An important difference is the fact that in the Ca-Si systems the metal $d$ orbitals are no longer the predominant states involved in the chemical bond with silicon. Figures 4–6 show that calcium $s$, $p$, and $d$ states contribute equally to the bonding interaction with silicon. Since the vertical-axis units are the same, the comparison is direct and gives evidence that both free-electron-like and localized Ca states are important in the bond with Si. In conclusion, the picture of the chemical bond in $Ca_2Si$ presents similarities and differences with the model proposed for late-transition-metal silicides. The atomiclike configuration of Si is also found in $Ca_2Si$, but the metal states involved in the bond with silicon, between $-3$ eV and $E_F$, are now formed by $s$-$p$-$d$ orbitals. Between the Fermi level and $+2$ eV we have the empty counterpart of the filled Ca—Si bonding structure.

We remark on the difference between the Ca(1) and Ca(2) PDSO's (Fig. 6). It is evident that Ca(1) has more $d$ states below $E_F$ than Ca(2), while the latter shows a more peaked PDOS above $E_F$. This result may be explained by looking at the different coordinations of the two atoms. Table II shows that Ca(1) must interact more strongly than Ca(2) with its Si neighbors because the first shell of Si atoms is closer. For this reason, the bonding structure below $E_F$ is stronger in the Ca(1) PDOS. Furthermore, Ca(1) interacts with two Ca neighbors at 3.63 Å, not found in the Ca(2) lattice. Therefore, in Ca(1) we expect a stronger $d$–metal-$d$ interaction and a wider and less

peaked PDOS above $E_F$.

Another striking feature of $Ca_2Si$ is due to the very low density of states at $E_F$ (Table IV). To investigate this aspect, we plot the energy bands along the symmetry directions of the Brillouin zone (Fig. 7). Figures 8 and 9 show that a direct energy gap of $\sim 1$ eV is always present along the BZ, but that the minimum of the "conduction band" near $T$ and in the $\Sigma, \Delta$ directions overlaps the Fermi energy, i.e., the energy of the highest occupied state, as in a semimetal.

The possible semimetal behavior of $Ca_2Si$ is quite interesting since it is known that metallic calcium under pressure undergoes a metal-semimetal transition.[57] The question that arises is whether the mechanism causing the transformation of pure Ca under pressure is related to the semimetallic behavior of $Ca_2Si$ at normal pressure. If the answer is positive, the main effect of the presence of Si is to reduce the average atomic volume of the crystal, simulating the effect of the pressure. Metallic calcium crystallizes in a fcc lattice with two valence electrons per cell. Therefore the metallic character is due to the overlap between the first band (nearly filled) and the second band (nearly empty). The major part of this overlap takes place in the $L-W$ direction, since the first band has an empty portion near $W$, with the $W_{2'}$ state of $d$ character unoccupied, and the second band presents the $L_{2'}$ state of $p$ character below $E_F$. The semimetal behavior of metallic Ca takes place when, upon reducing the interatomic distances, the $d$ band widens and the $W_{2'}$ $d$ state drops below $E_F$, while the $L_{2'}$ $p$ state rises at $E_F$.[54,55] When this happens, the first and the second band have no overlap and they only touch at one point along the symmetry line $L-W$. The state density at $E_F$ drops to zero and calcium turns into a semimetal. This transition is actually found in the experiments when the volume $V$ is reduced to $V \simeq \alpha V_0$, where $V_0$ is the normal-pressure atomic volume and $\alpha$ varies from 0.66 to 0.52.[57] The corresponding computed range for $\alpha$ is 0.78–0.54.[54] In calcium, $V_0 = 43.54$ Å$^3$/atom, and, therefore, from the experimental datum, we expect Ca to be a semimetal at atomic volumes between 28.73 and 22.64 Å$^3$/atom. Since in $Ca_2Si$ there are two different atoms and the crystal structure is quite complex, we are far from a simple picture based on two bands. Nevertheless, strong similarities may be found. The total number of Ca and Si atoms per $Ca_2Si$ cell is 12. An important simplification is possible if

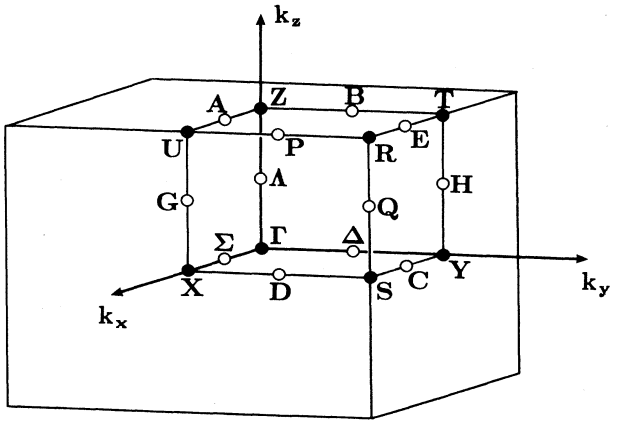


FIG. 7. Brillouin zone of the $Ca_2Si$ crystal lattice.

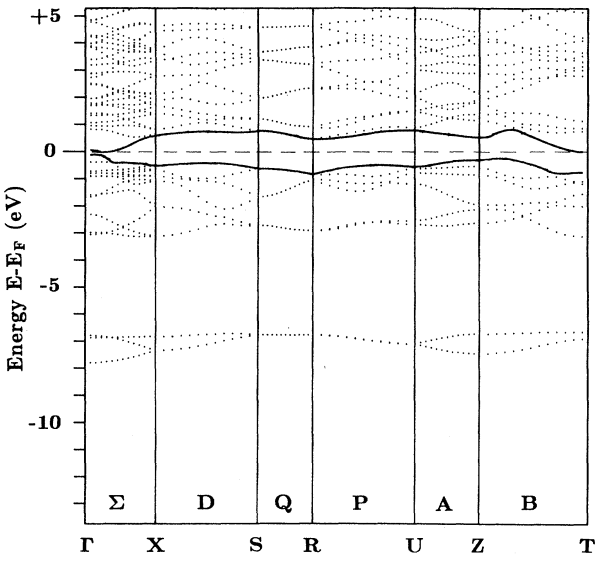


FIG. 8. Energy bands of $Ca_2Si$ along $\Sigma$-, $D$-, $Q$-, $P$-, $A$-, and $B$-symmetry lines. The highest occupied and lowest unoccupied states are indicated by solid lines.

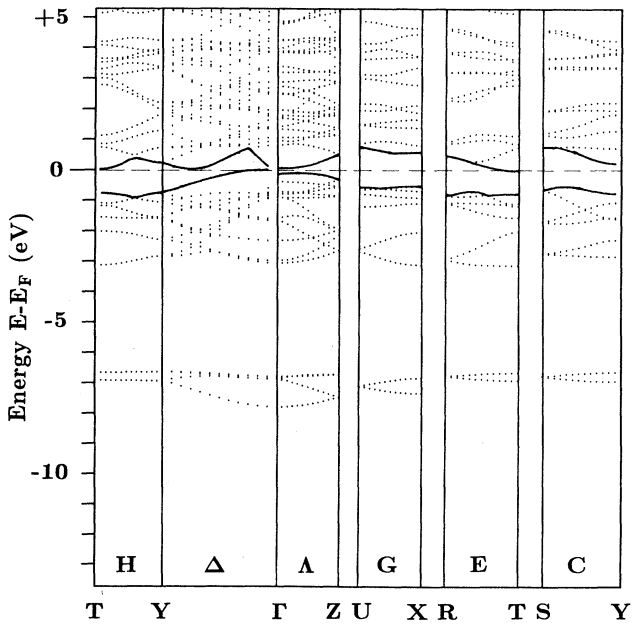


FIG. 9. Energy bands of $Ca_2Si$ along $H$-, $\Delta$-, $\Lambda$-, $G$-, $E$-, and $C$-symmetry lines. The highest occupied and lower unoccupied states are indicated by solid lines.

we treat the Si 3*s* states as core states. The reasons for this approximation have already been presented in discussing the data of Fig. 2. In such a simple picture both calcium and silicon contribute with two electrons per atom, the 4*s* and 3*p*, respectively, to the valence states. Therefore, we have 12 filled valence bands per cell. By considering the Si contribution similar to that of Ca, a drastic approximation that may be justified by the fact that we are in the Ca-rich silicide and that Si contributes with two valence electrons, we obtain one filled band per atom. In the same light, we evaluate an average atomic volume (volume of the cell divided by the total number of atoms) that turns out to be $V(Ca_2Si)=27.57$ Å$^3$/atom, just within the Ca semimetal range. The structure between $-3$ eV and $E_F$ in Fig. 1 corresponds to the first band in metallic Ca, now separated from the empty second band.

Further evidence of this interpretation comes out from the fact that the *d* band in $Ca_2Si$ is wider than that of metallic calcium, in spite of the smaller Ca concentration. As a matter of fact, the main *d* band extends up to $\sim+6$ eV above $E_F$ in normal Ca, to $\sim+8$ eV in Ca under pressure ($\alpha=0.51$),[55] and to $\sim+10$ eV in $Ca_2Si$ (paper II). This *d*-band widening is due both to the decrease of the average atomic volume and to the interaction of Si states with the Ca *d* orbitals. According to this interpretation, the presence of Si is sufficient to reduce the average interatomic distance, but not to remove the metal-semimetal transition. If the Si content is increased, we expect to lose this calciumlike behavior. This is what happens in CaSi, where the average atomic volume is still within the semimetal range, but the electronic structure is that of a metal. This analysis therefore provides evidence that the microscopic mechanism responsible for the metal-semimetal transition in $Ca_2Si$ and in Ca is similar, the presence of Si in the compound being equivalent to the effect of pressure in the pure metal.

### 2. *CaSi*

In the monosilicide the lower band is still mainly Si *s* in character, but the structure around $-6$ eV presents a significant Si *p* contribution (Figs. 2 and 3). This result indicates that the Si states evolve towards a single *s-p* band. In CaSi, as in $Ca_2Si$, the Ca states are slightly mixed with the Si *s* orbitals, which are now quite far from a corelike configuration. Even in this compound the Si *p* states mainly interact with Ca *s-p-d* orbitals. The structure between $-4$ and $-1$ eV is due to the bonding part of this interaction. In CaSi the Ca-Si interaction is stronger than in $Ca_2Si$ and the bonding structure is lowered in energy. This effect increases the number of Ca *d* electrons to 0.81 electron/atom and is indicative of an increased covalent interaction between Ca and Si upon increasing Si content.

The high-energy counterpart of the Ca—Si bonding structure found in $Ca_2Si$ is still present, but the Si weight is somewhat reduced. Furthermore, it is lowered in energy and located between $-1$ and $+2$ eV. This effect is responsible for the strong enhancement of the DOS at $E_F$ in CaSi.

### 3. *$CaSi_2$*

In the silicon-rich Ca silicide the Si *s* states occupy the lower part of a $\sim$12-eV filled band, with a predominant *p* character above $-4$ eV. An important feature consists of the different spectra of Si(1) and Si(2), due to the different environment. Figure 2 shows a difference of $\sim2$ eV in the bottom of the Si 3*s* states. It should be noticed that the absence of any feature in the Si(1) spectrum below $-10$ eV must not be taken literally. It is due to our large size of the Ca spheres and to the fact that the tails of the Si(2) wave functions are assigned to Ca states.

The analysis of the PDOS of $CaSi_2$, gives evidence of an extensive interaction between the Si *s-p* and Ca *s-p-d* states. All these states are involved in the chemical bond, and a single two-band model, like the Si *p*–metal-*d* coupling, is no longer appropriate. The bonding interaction is present at energies between $-4$ and $-1$ eV and reaches a maximum in this compound. The number of occupied *d* electrons is 0.87 electron/atom (Table IV).

As already found in $Ca_2Si$ and CaSi, the Ca-Si interaction gives rise to structures even above the Fermi level. The presence of different Si atoms can be related to different Ca-Si features: the structure at $\sim+2$ eV is mainly due to Ca-Si(2) coupling, while that around $+4$ eV is due to Ca-Si(1).

The high-energy part of the spectrum, as in CaSi, is characterized by a broad Ca-Si structure, extending from $+1$ to $+12$ eV (paper II). All Ca and Si orbitals are involved in this structure, where sometimes the features originate from the interaction of Ca with a single kind of Si. The main part of the *d* band ranges between $E_F$ and $+6$ eV with a peaked maximum around $+5.5$ eV. These results may be compared with the outcomes of a tight-binding calculation of the $CaSi_2$/Si(111) interface.[58] The comparison gives evidence of significative differences in various features in the location of the main peak of the *d* band, which, in this semiempirical calculation, is found around $+3$ eV. These differences may arise from the different electron properties of the interface or, more likely, from the approximations of the tight-binding Hamiltonian.

The different behavior of the Si(1) and Si(2) PDOS's is a fingerprint of the presence of an ionic component in the Ca—Si. Besides the covalent character of the Si—Ca bond, common to the other Ca silicides and due to the mixing of Ca and Si orbitals, as discussed up to now, we find that some ionic component is present in the bond of this compound. This effect can be recognized by a rigid shift of $\sim2$ eV of the eigenvalues of Si(1) with respect to Si(2). The $V(r)$ curves of Fig. 10 show a continuous trend in the potential strength upon varying Si content, with the exception of Si(1) in $CaSi_2$. In this case the potential is more repulsive by $\sim2$ eV with respect to that of Si(2). This fact is responsible for the well-defined features of the density of states. The bottom of Si(1) starts at $\sim-10$ eV, while that of Si(2) starts at $\sim-12$ eV. In the empty part of the spectrum the Si(2) *p* states are peaked around $+2$ eV, leading to a $Si^2p$–Ca *d* structure that has been observed in bremsstrahlung isochromat spectra[34] and in inverse photoemission (paper II). It should be no-

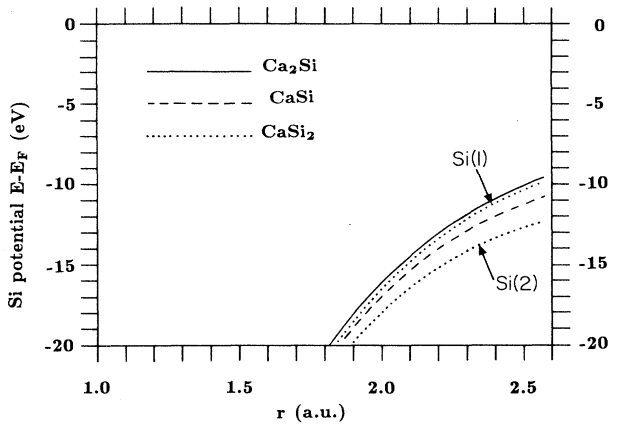


FIG. 10. Self-consistent LMTO ASA crystal potential within Si spheres in Ca silicides. Energies are in eV, relative to $E_F$.

ticed that the distribution of the filled Si $p$ states is not significantly different in the inequivalent Si atoms of $CaSi_2$. We believe that this is due to the bonding interaction with the calcium $s$-$p$-$d$ states that stabilize the Si $p$ states in the energy range between $-4$ and $-1$ eV.

The main difference between Si(1) and Si(2) coordination is the Ca atom found at a distance of 3.11 Å from Si(1), but missing in the Si(2) lattice. As a consequence, Si(1) has four Ca neighbors, while Si(2) has only three. We may explain the difference between the Si(1) and Si(2) PDOS's by assuming that some charge transfer from Ca to Si takes place. Since the Ca coordination of Si(1) is higher, the net amount of charge found on the Si(1) atom is greater than that on the Si(2) site and the potential of Si(1) is more repulsive. We note that if the bond would be covalent only, the greater coordination of Si(1) would produce a gain in energy for the bonding states found at the bottom of the valence band, the opposite of the result shown in Fig. 2. This result may suggest some ionic component, even for the bond of the other Ca silicides. Any attempt to quantify the extent of ionicity depends crucially on the particular definition adopted (see the discussion in Sec. V). Our results show that in Ca silicides both covalent and ionic features are present and that neither covalency nor ionicity alone may characterize the chemical bond.

## VI. EXPERIMENTAL RESULTS AND COMPARISON WITH THE CALCULATIONS

In this section we present the photoemission measurements on valence electrons and compare the theoretical results with the experiments.

The main experimental basis is provided by the valence spectra measured at 150 eV and summarized in the upper panel of Fig. 11. This photon energy is very convenient since the photoemission cross sections for $s$-$p$ and $d$ contributions are roughly of the same order (within a factor of 2) as far as one can say from the present knowledge of photoionization cross sections.[59] Thus, a direct comparison between the measured and calculated DOS's is a reasonable approximation, and more accurate evaluations of matrix elements are not required in the present discussion. Besides, we do the usual approximation of neglecting the $k$-selection-rule effect; this is fully reasonable at these energies in photoemission from polycrystals. Before proceeding to a comparison with the calculations, we note that in $Ca_2Si$ and CaSi a weak feature appears at $-5$ eV; this is due to the small fraction of sample area that is not perfectly clean, as discussed in Sec. IV, and therefore has no counterpart in the calculations. We stress again that the presence of this feature does not prevent a meaningful comparison between theory and experiment.

In order to compare theory with experiment, it is necessary to take into account the effects of experimental broadening and of the presence of secondary electrons in the measurements. The calculated DOS's shown in Fig. 1 have been broadened with a Lorentzian whose width parameter is equal to $[0.1+0.12(E_F-E)]$ eV, where $E_F-E$

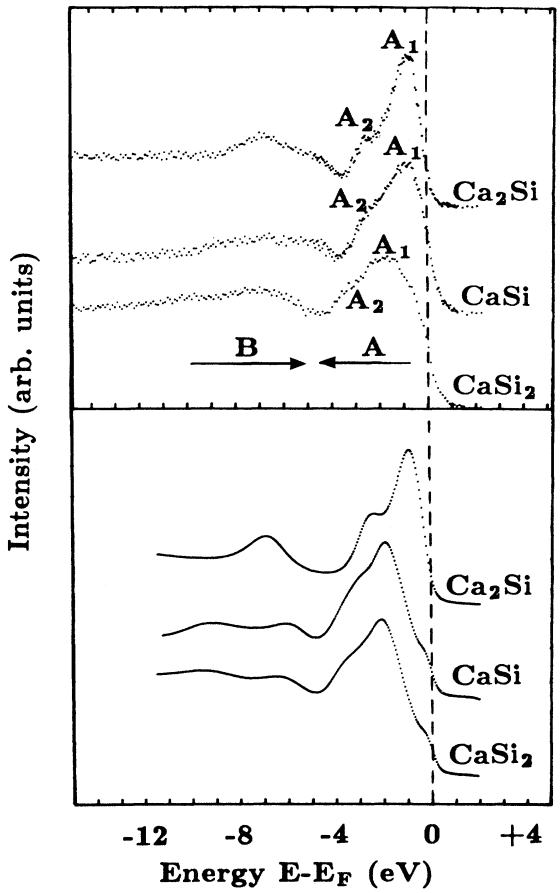


FIG. 11. Comparison between measured and computed photoemission spectra in the whole family of Ca silicides; the trends across the family are pointed out. Upper panel: angle-integrated spectra measured at 150 eV photon energy. Lower panel: theoretical spectra calculated as explained in the text starting from the theoretical density of states.

is the energy of the hole measured from the Fermi level. The instrumental broadening has been represented with a Gaussian having 0.4 eV total width at half-height. This combination of parameters turned out to be satisfactory; around these values other combinations can also be used, but since our discussion is independent of this choice there is no need to carry out a detailed investigation of this particular subject. To retain a better evidence of the computed features, we have used a slightly smaller broadening than that needed to give a perfect simulation near the Fermi level, where in the measurements we do not pick up the weak shoulder seen in the calculations for CaSi and $CaSi_2$. The presence of secondary electrons can be taken into account in a simple approximation way by adding a linear background increasing from $E_F$.

Theoretical spectra obtained by this procedure are collected in the lower panel of Fig. 11. The comparison between theory and experiment can be done in the following way.

(i) The main features of the theoretical spectra are in perfect agreement with experiment. In particular, the spectra are clearly divided into two regions: a peaked region between $-4$ eV and $E_F$ (identified with $A$ in Fig. 11) containing, as stated above, most of the Ca *s-p-d* contribution besides the Si mostly *p* contribution, and a higher-binding-energy structure, strongly varying with stoichiometry, where the dominant weight comes from the Si *s* states ($B$ in Fig. 11). Upon passing from $Ca_2Si$ to $CaSi_2$, the trend, both in the measurements and in calculations, is a very clear widening of the peak $A$, which is due to the increased Ca-Si interaction when the system becomes richer in Si. Another important feature of the theoretical results, clearly seen in Fig. 2, is that only in $Ca_2Si$ are the Si *s* states split off with respect to the other states. This is clearly confirmed by the experiments, since only in this case does one see a clear peak in region $B$. In the other silicides the theoretical distribution of states, due to the formation of a Si *s-p* band, is much broader in this region and the details could not be identified in the measurements due to noise problems. One can conclude that all the gross features of the measurements are well reproduced by the calculations.

(ii) The quality of the calculations is better investigated by a direct comparison between theory and experiment in each silicide. To help this analysis, we compare for each silicide theory and experiment in Fig. 12. By focusing the discussion on region $A$, it is clear that the agreement between theory and experiment is excellent in the two extreme compounds of the phase diagram ($Ca_2Si$ and $CaSi_2$); in particular, the position of peak $A_1$ and the presence of shoulder $A_2$, which becomes a distinct feature in $Ca_2Si$, are very well reproduced. Region $A$ is less satisfactory in the calculations for CaSi. Also, in this case the main features are clearly reproduced by the calculations (Fig. 12), but the computed main peak is $\sim 0.9$ eV below the experimental value. We note that this disagreement is not due to neglect of the photoemission matrix elements that may weight the various orbital contributions differently from the total DOS; from the data shown in Figs. 2–6 it is clear that no combination of partial contributions can produce a good agreement with the experimental data. Thus, at least, the greatest fraction of this 0.9-eV difference must be regarded a true inadequacy of the calculated states which, on the other hand, are fully satisfactory in the other respects.

An error of the order of 1 eV is not surprising because the expected accuracy of our band-structure calculation is of this order. This is mainly due to the atomic-sphere approximation (ASA), which is responsible for uncertainties up to $\sim 1$ eV in the eigenvalues of the filled states, as shown in Fig. 6 of Ref. 19. We notice that a similar result has been obtained by the investigation of transition-metal silicides,[18] where good agreement between x-ray photoemission measured and computed spectra is found for a variety of Si-rich silicides, except for the monosilicides, where a disagreement of $\sim 1$ eV was found.

According to our view, the much better agreement found in $Ca_2Si$ and $CaSi_2$ is fortuitous since the accuracy of our single-particle calculation is within 1 eV. We will see in paper II that the major discrepancy between measured and computed spectra is reached in the metal-rich silicide $Ca_2Si$. In the study of empty states both self-energy effects (present in all compounds) and approxima-

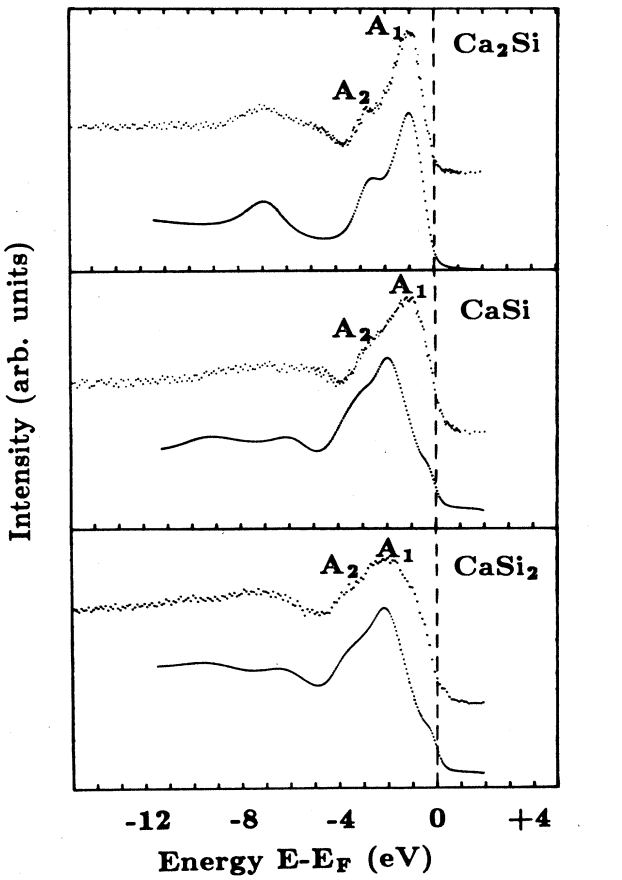


FIG. 12. Comparison between measured and computed photoemission spectra for each Ca silicide; the spectra are the same as in Fig. 11.

tions of the single-particle calculations (ranging from 0 to less than 1 eV) are necessary to interpret the spectra, unlike the case of filled states, where no evidence of a self-energy effect is found.

(iii) The different nature of the electron states of $Ca_2Si$ with respect to the other two silicides is evident from our calculations, which show that $Ca_2Si$ is a semimetal while the other two silicides are metallic. The reader is referred to Table IV and to the discussion concerning Fig. 1 and Figs. 8 and 9. A direct proof of the semimetallic behavior of $Ca_2Si$ based on transport measurements or on Fermi-surface analysis is lacking, to the best of our knowledge. In this respect, valence-band photoemission cannot be quantitative; nevertheless, very strong qualitative support comes from the present photoemission results. In effect, the endpoint of the spectra of $Ca_2Si$ is different with respect to the other two silicides, which, on the other hand, have the same endpoint; this is shown clearly in Fig. 13, which gives an extrapolated upper edge of $Ca_2Si$ $\sim 0.35$ eV lower than CaSi and $CaSi_2$. This value is of the order of the experimental linewidth, as must be the case in a comparison of a semimetal and of a metal photoemission spectrum. Moreover, the position of the extrapolated edge of $Ca_2Si$ is coincident with the Fermi edge positioned experimentally at the half-height of the Fermi step of gold; also, this fact is consistent with the semimetallic nature of $Ca_2Si$.

(iv) The presence of a covalent component of the chemical bond is shown in the theoretical results by the fact that the Ca and Si PDOS's give contributions to the total DOS which are very similar in shape. This point is very important, and the experimental evidence supporting this picture is given here. To discuss this point, it is convenient to consider the shape of the theoretical Ca and Si PDOS's in the three silicides after broadening is done as explained above. This comparison is done for the three silicides in Fig. 14, where the Ca and Si contributions in arbitrary units are normalized to the same height in order to put in evidence the overall shape similarity. Since, as we already noticed, we do not resolve the shoulder present in CaSi and in $CaSi_2$ near the Fermi level, we have to focus our attention on the higher-binding-energy region, i.e., on the left side of the main peak $A$. Only in the $CaSi_2$ case is there an appreciable difference in the two contributions in the energy interval between $\sim -2.5$ and $-5$ eV. Thus, in a series of measurements in which the relative weight of the Ca and Si contributions are

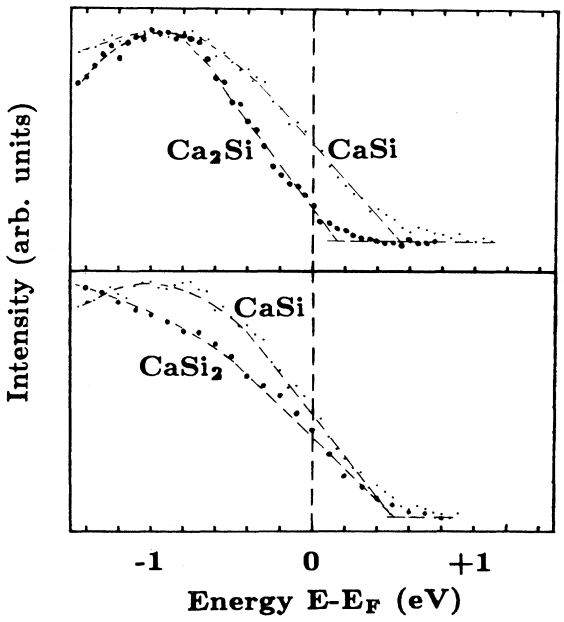


FIG. 13. Expanded view of the endpoint region of the measured spectra. Note that the monosilicide and the disilicide have the same extrapolated endpoint, while $Ca_2Si$ has the shape of the spectrum which gives rise to an extrapolated endpoint at lower energy; the Fermi level is measured with a gold sample. The difference in the extrapolated endpoints comes from density of states having different shapes for systems having aligned Fermi levels.

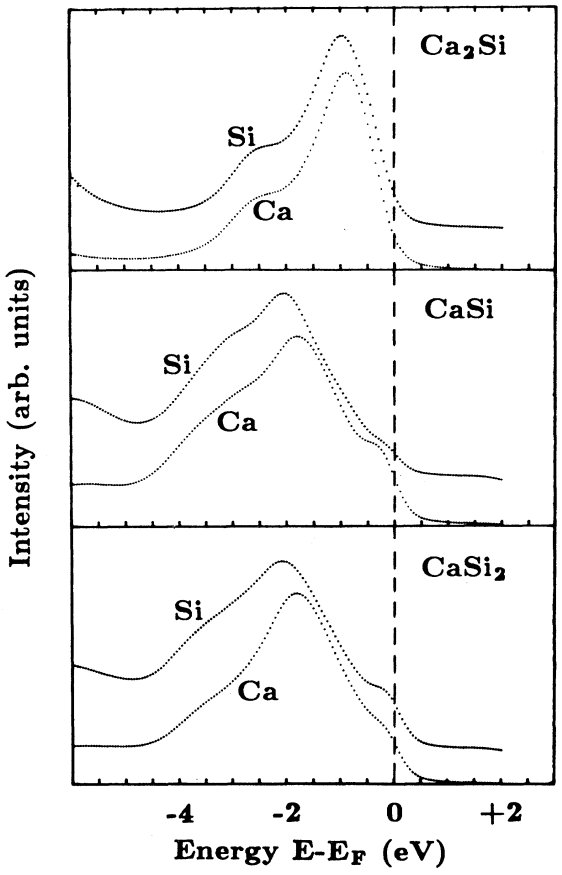


FIG. 14. Calculated contributions from Si and Ca to the total density of states of the three silicides, calculated from the theoretical density of states by taking into account the broadening due to the lifetime and to the instrumental resolution. The broadening parameters are specified in the text.

modified, no change in the spectra is expected within the experimental sensitivity for $Ca_2Si$ and CaSi, whereas an effect should be seen in $CaSi_2$. This is exactly what is found experimentally, thus confirming the above theoretical picture. This experimental evidence is based on the resonant valence photoemission at the crossing of the Ca $L_{2,3}$ threshold ($\sim$350 eV); in this way the Ca contribution is strongly enhanced, so that relative [Ca]/[Si] weight is increased with respect to the spectra at 150 eV used so far (we have estimated an increase by an order of magnitude). These resonant photoemission spectra are very difficult to measure since the energy is above the $K$ edge of carbon, which is a contaminant of the optical elements. In spite of this and of the consequent high noise, the resonant spectra are good enough to confirm the theoretical picture. In particular, the spectra at the $L_{2,3}$ threshold (Fig. 15) are very similar to those at 150 eV for $Ca_2Si$ and CaSi, whereas a rather distinct effect is seen in $CaSi_2$, with a narrowing at the resonance in excellent agreement with that predicted by theory. In the resonant spectrum of $Ca_2Si$ we do not see the feature at 3 eV (called $A_2$ in the preceding figures); this is probably due to the high noise of the measurements, and this point cannot be discussed.

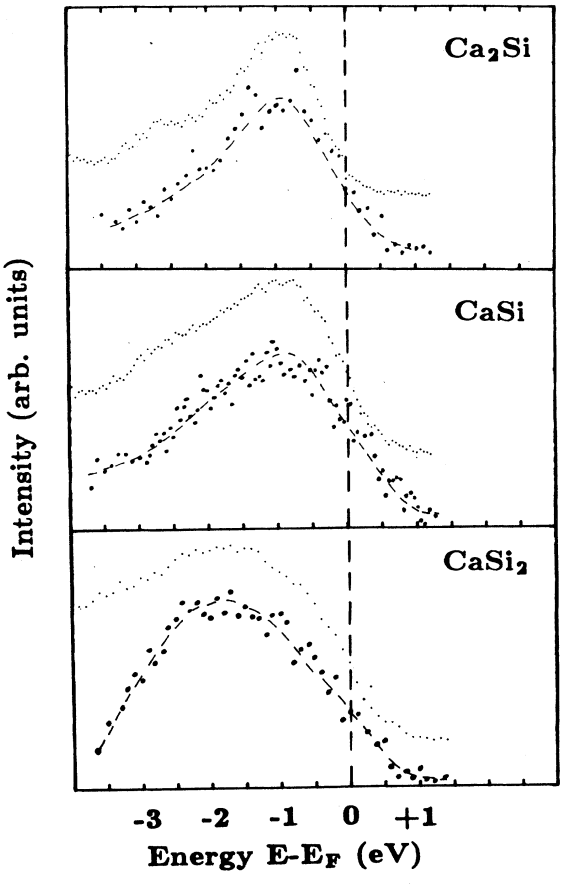


FIG. 15. Comparison between the upper valence photoemission from the three silicides at 150 eV (small dots) and at 350 eV just above the $L_{2,3}$ threshold of calcium (large dots). Within the statistical noise the general shape of the spectra is the same in $Ca_2Si$ and in CaSi, while a clear difference is seen in $CaSi_2$.

As a final point, we observe that our calculations may be used to investigate some feature of the Ca-Si–interface photoemission spectra.[21] These data show that the interface reaction produces a lowering of the Ca $d$ states just below $E_F$ and a new feature at $\sim -1.4$ eV. According to our analysis, this finding is due to the Ca-Si interaction which increases the Ca $d$ occupancy. As a net result the Ca-filled $d$ states do not belong to the tail of the empty main $d$ band, as in pure Ca, but form a bonding structure well separated from the main $d$ band. The main peak of this structure varies with Ca-Si interaction from $\sim -1$ eV in $Ca_2Si$ to $\sim -2$ eV in $CaSi_2$.

## VII. CONCLUSIONS

We present a joint theoretical and experimental investigation of the electron properties of $Ca_2Si$, CaSi, and $CaSi_2$. The densities of states have been evaluated by the LMTO ASA method, while the experimental spectra are based on synchrotron-radiation photoemission. The photoemission spectra have been collected in different frequency regimes: at $h\nu=150$ eV, where the $s$-$p$ and $d$ cross sections are similar, and at $h\nu=350$ eV, under resonant photoemission conditions at the Ca $L_{2,3}$ threshold.

A detailed comparison between theory and experiment has been performed and many features of the electron properties and of the chemical bond in these compounds have been understood. The general result is that ground-state DOS's provide an excellent tool to investigate the photoemission spectra of these systems. The overall agreement across the whole silicide family is very satisfactory and is within 1 eV, while for $Ca_2Si$ and $CaSi_2$ it is much better. The same results will be used in paper II to interpret inverse photoemission spectra on the same samples. We will show that all the main features present in the empty-state experimental spectra can be consistently described.

The main conclusions of this investigation are the following.

(i) The chemical interaction between Ca and Si cannot be interpreted simply in terms of covalent or ionic bonds. The covalent or ionic character depends critically on space partitioning which, for such complex compounds, cannot be defined unambiguously. We have found that covalent character is present together with some ionic contribution.

(ii) The orbital origin of the covalent contribution to the bond depends on the stoichiometry. While in $Ca_2Si$ the Si states involved in the mixing with Ca are mainly $3p$, upon increasing the Si content Si $3s$ orbitals are promoted to form an unique $s$-$p$ band. All the Ca $s$-$p$-$d$ states strongly interact with Si states. This result is different from what is found in late transition-metal silicides, where the metal states involved in the mixing with Si are mainly the $d$ orbitals.

(iii) The strength of the Si-Ca interaction increases with Si concentration and is responsible for the increasing number of filled Ca $d$ states upon going from $Ca_2Si$ to $CaSi_2$. This effect is responsible for the variations of the

bonding structure below $E_F$.

(iv) The complex structure of these compounds, with nonequivalent Ca atoms in $Ca_2Si$ and nonequivalent Si atoms in $CaSi_2$, has direct consequences on the features of the density of states. Many structures can be correlated to interactions localized on a quite distinct Ca-Si pair.

(v) The metal-rich silicide is found to be a semimetal. This theoretical result, which is suggested to have the same origin of the semimetal transition of pure Ca under pressure, is consistent with a careful analysis of the photoemission spectra near the Fermi level.

## ACKNOWLEDGMENTS

We are grateful to C. Calandra, J. C. Fuggle, F. Manghi, M. Sancrotti, D. D. Sarma, and W. Speier for stimulating discussions. Part of this work has been done at SSRL (Stanford Synchrotron Radiation Laboratory), which is supported by the U.S. Department of Energy. Financial support by Consiglio Nazionale delle Ricerche (Italy) and Ministero della Pubblica Istruzione (Italy) is acknowledged. Calculations have been performed at the Computer Center (Centro di Calcolo Elettronico) of the University of Modena.

---

*Permanent address: Istituto di Fisica, Politecnico di Milano, piazza Leonardo da Vinci 32, I-20133 Milano, Italy.

†Permanent address: Institut für Festkörperforschung der Kernforschungsanlage Jülich, D-5170 Jülich, West Germany.

[1]P. S. Ho, G. W. Rubloff, J. E. Lewis, V. L. Moruzzi, and A. R. Williams, Phys. Rev. B **22**, 4784 (1980).

[2]O. Bisi and C. Calandra, J. Phys. C **14**, 5479 (1981).

[3]G. Rossi, I. Abbati, L. Braicovich, I. Lindau, and W. A. Spicer, Solid State Commun. **39**, 195 (1981).

[4]I. Abbati, L. Braicovich, B. De Michelis, O. Bisi, and R. Rovetta, Solid State Commun. **37**, 119 (1981).

[5]K. L. I. Kobayashi, S. Sugaki, A. Ishizaka, Y. Shiraki, H. Daimon, and Y. Murata, Phys. Rev. B **25**, 1377 (1982).

[6]G. Rossi, I. Abbati, L. Braicovich, I. Lindau, and W. E. Spicer, Phys. Rev. B **25**, 3627 (1982).

[7]P. J. Grunthaner, F. J. Grunthaner, and A. Madhukar, J. Vac. Sci. Technol. **20**, 680 (1982).

[8]G. W. Rubloff, in *Festkörperprobleme (Advances in Solid State Physics)*, edited by P. Grosse (Vieweg, Braunschweig, 1983), Vol. 23, p. 179.

[9]Yu-Jeng Chang and J. L. Erskine, Phys. Rev. B **28**, 5766 (1983).

[10]K. Tanaka, T. Saito, K. Suzuki, and R. Hasegawa, Phys. Rev. B **32**, 6853 (1985).

[11]O. Bisi and L. W. Chiao, Phys. Rev. B **25**, 4943 (1982).

[12]A. Franciosi and J. H. Weaver, Surf. Sci. **132**, 324 (1983).

[13]J. H. Weaver, A. Franciosi, and V. L. Moruzzi, Phys. Rev. B **29**, 3293 (1984).

[14]C. Calandra, O. Bisi, and G. Ottaviani, Surf. Sci. Rep. **4**, 271 (1984).

[15]D. M. Bylander, L. Kleinman, K. Mednick, and W. R. Grise, Phys. Rev. B **26**, 6379 (1982); B. K. Bhattacharyya, D. M. Bylander, and L. Kleinman, *ibid.* **32**, 7973 (1985).

[16]J. Tersoff and D. R. Hamann, Phys. Rev. B **28**, 1168 (1983).

[17]O. Bisi, O. Jepsen, and O. K. Andersen, Phys. Rev. B **36**, 9439 (1987).

[18]W. Speier, E. v. Leuken, J. C. Fuggle, D. D. Sarma, L. Kumar, B. Dauth, and K. H. Buschow, Phys. Rev. B **39**, 6008 (1989).

[19]O. K. Andersen, Phys. Rev. B **12**, 3060 (1975).

[20]C. Chemelli, M. Sancrotti, L. Braicovich, F. Ciccacci, O. Bisi, A. Iandelli, G. L. Olcese, and A. Palenzona, this issue, the following paper, Phys. Rev. B **40**, 10 210 (1989).

[21]A. Franciosi, J. H. Weaver, and D. T. Peterson, Phys. Rev. B **31**, 3606 (1985).

[22]L. Braicovich, in *The Chemical Physics of Solid Surfaces and Heterogeneous Catalysis*, edited by D. A. King and D. P. Woodruff (Elsevier, Amsterdam, 1988), Vol. 5, p. 266.

[23]G. Rossi, Surf. Sci. Rep. **7**, 1 (1987), and references therein.

[24]M. Sancrotti, I. Abbati, A. Rizzi, L. Calliari, F. Marchetti, and O. Bisi, Surf. Sci. **189/190**, 300 (1987).

[25]M. Sancrotti, A. Rizzi, and F. Marchetti, Phys. Rev. B **37**, 3120 (1988).

[26]J. F. Morar and M. Wittmer, Phys. Rev. B **37**, 2618 (1988), J. Vac. Sci. Technol. **A6**, 1340 (1988).

[27]I. Abbati, L. Braicovich, U. Del Pennino, S. Nannarone, G. Rossi, and I. Lindau, Surf. Sci. **162**, 645 (1985).

[28]R. Baptist, A. Pellisier, and G. Chauvet, Solid State Commun. **68**, 555 (1988).

[29]U. O. Karlsson, F. J. Himpsel, J. F. Morar, F. R. McFeely, D. Rieger, and J. A. Yarmoff, Phys. Rev. Lett. **57**, 1247 (1986).

[30]M. A. Olmstead, R. I. G. Uhrberg, R. D. Bringans, and R. Z. Bacharach, Phys. Rev. B **35**, 7526 (1987).

[31]J. L. Batstone, J. M. Phillips, and E. C. Hunke, Phys. Rev. Lett. **60**, 1394 (1988).

[32]R. M. Tromp and M. C. Reuter, Phys. Rev. Lett. **61**, 1756 (1988).

[33]A. Spinsanti, O. Bisi, I. Abbati, L. Braicovich, A. Iandelli, G. L. Olcese, A. Palenzona, C. Carbone, and I. Lindau, in Proceedings of the European Workshop on Refractory Metals and Silicides (Aussois, 1987) [Suppl. Le Vide Les Couches Minces **42**, 211 (1987)].

[34]D. D. Sarma, W. Speier, L. Kumar, C. Carbone, A. Spinsanti, O. Bisi, A. Iandelli, G. L. Olcese, and A. Palenzona, Z. Phys. B **71**, 69 (1988).

[35]M. Sancrotti, I. Abbati, L. Calliari, F. Marchetti, O. Bisi, A. Iandelli, G. L. Olcese, and A. Palenzona, Phys. Rev. **37**, 4805 (1988).

[36]W. B. Pearson, *Handbook of Lattice Spacing and Structures of Metals and Alloys* (Pergamon, New York, 1958).

[37]H. L. Skriver, *The LMTO Method* (Springer-Verlag, Berlin, 1984).

[38]D. Glötzel, B. Segall, and O. K. Andersen, Solid State Commun. **36**, 403 (1980).

[39]A. K. McMahan, Phys. Rev. B **30**, 5835 (1984).

[40]J. Keller, J. Phys. C **4**, L85 (1971).

[41]Xu Jian-hua and Xu Yong-nian, Solid State Commun. **55**, 891 (1985).

[42]W. R. L. Lambrecht, Phys. Rev. B **34**, 7421 (1986).

[43]O. Bisi, L. Braicovich, C. Carbone, I. Lindau, A. Iandelli, G. L. Olcese, and A. Palenzona (unpublished).

[44]P. Hohenberg and W. Kohn, Phys. Rev. **136**, B864 (1964).

[45]W. Kohn and L. J. Sham, Phys. Rev. **140**, A1133 (1965).

[46]L. Hedin and B. I. Lundqvist, J. Phys. C **4**, 2064 (1971).

[47]O. Jepsen and O. K. Andersen, Solid State Commun. **9**, 1763 (1971).

[48]V. L. Moruzzi, J. F. Janak, and A. R. Williams, *Calculated Electronic Properties of Metals* (Pergamon, New York, 1978).

[49]H. L. Skriver, Phys. Rev. B **31**, 1909 (1985).

[50]N. E. Christensen, Phys. Rev. B **32**, 207 (1985).
[51]K. A. Gschneidner, in *Solid State Physics,* edited by F. Seitz, D. Turnbull, and H. Ehrenreich (Academic, New York, 1964), Vol. 16, p. 275.
[52]O. Kubaschewski and H. Villa, Z. Elektrochem. **53**, 32 (1949).
[53]S. R. Nagel, U. M. Guber, C. F. Hague, J. Krieg, R. Lapka, P. Oelhafen, H. J. Güntherodt, J. Evers, A. Weiss, V. L. Moruzzi, and A. R. Williams, Phys. Rev. Lett. **49**, 575 (1982).
[54]J. P. Jan and H. L. Skriver, J. Phys. F **11**, 805 (1981).
[55]J. W. McCaffrey, J. R. Anderson, and D. A. Papaconstantopoulos, Phys. Rev. B **7**, 674 (1973).
[56]O. K. Andersen, in *The Electronic Structure of Complex Systems,* edited by P. Phariseau and W. A. Temmerman (Plenum, New York, 1984).
[57]R. A. Stager and H. G. Drickamer, Phys. Rev. **131**, 2524 (1963).
[58]Xu Yongnian, Zhang Kaiming, and Xie Xide, Phys. Rev. B **33**, 8602 (1986).
[59]J. J. Yeh and I. Lindau, At. Data Nucl. Data Tables **32**, 1 (1985).